Journal of Structural Geology 31 (2009) 776–790

Contents lists available at ScienceDirect

Journal of Structural Geology

journal homepage: www.elsevier.com/locate/jsg

Transposed high-pressure granulite fabrics (Cabo Ortegal, NW Spain): Implications on the scales of deformation localization

P. Puelles [a,*], B. Ábalos [a], J.I. Gil Ibarguchi [b]

[a] Departamento de Geodinámica, Universidad del País Vasco, PO Box 644, E-48080 Bilbao, Spain
[b] Departamento de Mineralogía y Petrología, Universidad del País Vasco, PO Box 644, E-48080 Bilbao, Spain

ARTICLE INFO

Article history:
Received 11 November 2008
Received in revised form
21 April 2009
Accepted 1 May 2009
Available online 13 May 2009

Keywords:
Ductile shear zones
Deformation mechanisms
Localization
Transposition
EBSD
Cabo Ortegal
NW Spain

ABSTRACT

High-pressure granulite facies rocks of the Bacariza Formation (Cabo Ortegal, NW Spain) were syn-metamorphically deformed at the contacts with the bounding units (peridotite and eclogite massifs). This enabled the formation of meter-thick, spectacular shear zones with reworked and transposed foliations and lineations. The texturally stable mineral assemblage of the new fabrics records an intense, ductile deformation of the mineral aggregate at temperatures of 700–800 °C associated with amalgamation of eclogite, high-pressure granulitic rocks and ultramafic sheets in deep portions of a subduction channel. The lattice preferred orientation of the main constituent minerals (garnet, augite, amphibole, plagioclase, quartz and biotite) discloses the active deformation mechanisms at the scale of the mineral grains and the relationships with the deformation at larger scales. Overprinting relationships of the metamorphic assemblages demonstrates that partitioning and deformation localization occurred at different scales under similar high-grade conditions. Complete macroscopic transposition in the shear zones was complementary to meso and microscopic partitioning of deformation intensity and mechanisms between different lithological layers and mineral species.

1. Introduction

The burial, metamorphism, internal deformation and exhumation of shallow crustal units in subduction zones have been the focus of detailed studies in recent years (e.g. Ernst, 2006). Numerical and mechanical analogues have been employed to that end, as well as inductive and deductive perspectives integrating metamorphic and structural studies (Chemenda et al., 2000; Burov et al., 2001; Gerya et al., 2002, 2008). It is generally assumed that high-pressure metamorphic units or terranes are formed in such subduction settings, from which they were incorporated into orogens and exhumed to the Earth's surface at either fast or slow plate-tectonic velocities, according to many geochronological and petrological studies (Amato et al., 1999; Hacker et al., 2003; Kylander-Clark et al., 2008; Yamato et al., 2008). Of a different nature is, however, the progress achieved in the recognition and understanding of the tectonic imprint recorded by the rocks that underwent such evolutions (e.g. Hacker and Gans, 2005). It has been demonstrated that crustal rocks can be buried to mantle depths (and then exhumed) without internal deformation (e.g.: Gil Ibarguchi, 1995; Tilton et al., 1997; Wallis et al., 1997). Partitioning of deformation is thus implied, the movement zones occurring somewhere outside, though they are expected to have accommodated intense deformations and tectonic displacements of several tens to hundreds of kilometres. Greenschists facies shear zones are often identified in the field bounding the high-pressure rocks (e.g.: Bousquet, 2008). They indicate a metamorphic gap that, in our view, should be also structural, though usually this is not so evident. The metamorphic contrast is interpreted as if the bounding shear zones were late structures (e.g. as discussed by Ganne et al., 2006), not directly related to the high-pressure structures. In spite of this, a significant part of the tectonic displacements necessarily occurred at deep crustal or upper lithospheric mantle conditions. Very few studies have given undisputed evidence on the structures and fabrics formed in those settings (e.g.: Boundy et al., 1992; Kurz et al., 1998; Foreman et al., 2005) and it is striking that no evidence is preserved of such extreme events.

Microstructural studies of high-pressure minerals and fabrics constitute an important source of information on the rheology and deformation conditions at deep parts of subduction zones (Jin et al., 2001; Terry and Robinson, 2004; Kurz, 2005). High-pressure mineral assemblages are often identified without dispute. However, understanding high-pressure fabrics in the same rocks is not so straightforward (Lenze et al., 2005; Lenze and Stöckhert, 2007),

* Corresponding author. Tel.: +34 4 6015377; fax: +34 4 6012470.
E-mail address: pablo.puelles@ehu.es (P. Puelles).

0191-8141/$ – see front matter © 2009 Elsevier Ltd. All rights reserved.
doi:10.1016/j.jsg.2009.05.001

unless they are mono- or bimineralic. Techniques such as Electron Back-Scattered Diffraction (EBSD) have triggered a rapid increase in the number of microstructural and textural studies on these and other related topics. Among the constituent minerals of high-pressure rocks, particular attention has been devoted to garnet, omphacitic clinopyroxene, rutile and quartz (Mauler et al., 2001; Bascou et al., 2002; Egydio-Silva et al., 2002; Storey and Prior, 2005; Vollbrecht et al., 2006; Neufeld et al., 2008; Toy et al., 2008; Whitney et al., 2008).

We present a detailed microstructural study of a ductile shear zone at the contact between a high-pressure mafic granulite nappe (the Bacariza Formation of the Cabo Ortegal Complex, NW Spain; Fig. 1a) and a structurally underlying eclogite massif. The petrographic, structural, thermobarometric and geochronological data available (Ábalos et al., 2003; Puelles, 2004; Puelles et al., 2005a) show that the high-pressure granulite facies metamorphism differs from that of regional granulite terranes of medium to low pressure (with long residence times in deep crustal settings; e.g.: Bohlen, 1991). It would actually reflect a unique P–T loop (e.g.: O'Brien and Rötzler, 2003) related to eo-Hercynian subduction. In this study the microstructures and fabrics of garnet, augite, quartz, plagioclase, amphibole and biotite of a transposed granulitic tectonite are described and measured. The results obtained enable us to characterize ductile deformation at deep crustal levels and discuss the structural imprint at various scales of the tectonic amalgamation of Cabo Ortegal highest-pressure nappes in a subduction channel subsequent to peak high-pressure metamorphism.

2. Geological context and sample description

2.1. Geological setting

The Cabo Ortegal Complex is one of the Allochthonous Complexes of the northwestern Iberian Massif (Fig. 1a). The Complexes represent fragments of variably subducted continental and oceanic lithosphere that were obducted onto the Gondwana edge during the Variscan orogeny (Martínez Catalán et al., 1997). They comprise a Lower Allochthon at the bottom, a sandwiched ophiolitic complex, and an Upper Allochthon on top (Fig. 1a). The Upper Allochthon of the Cabo Ortegal Complex contains eclogites, high-pressure granulite facies lithologies, metaperidotites, metagabbros, metaserpentinites and various types of gneisses (Vogel, 1967; Peucat et al., 1990; Gil Ibarguchi et al., 2000). Its primary structure is related to middle Devonian (Schäfer et al., 1993; Ordóñez et al., 2001), high-pressure and high-temperature tectonic events. An ultramafic sheet formed by the Limo, Herbeira and Uzal massifs (Girardeau et al., 1989; Santos Zalduegui et al., 2002) rests on high-pressure granulite facies rocks, these on a km-scale eclogite massif, and the whole ensemble (Fig. 1b) on high-pressure gneisses. All these units are separated by ductile thrust contacts (Ábalos et al., 1994).

The high-pressure granulite facies Bacariza Formation outcrops in the central part of the Cabo Ortegal Complex (Fig. 1b) and constitutes a heterogeneous suite dominated by garnet- and plagioclase-rich lithotypes (Puelles, 2004) such as mafic granulite or plagio-pyrigarnite (G1 in the Fig. 1b), intermediate to felsic plagioclase-rich granulite (G2), Mg-rich mafic granulite (G3), ultramafic granulite or pyrigarnite (G4) and granulitic orthogneiss (G5). On the basis of the microstructural and petrographic criteria, a high-pressure deformational event can be recognized that, in detail, was a polyphasic episode consisting of two phases of deformation, D1 and D2 (Ábalos et al., 2003). D1 promoted the development of penetrative S1–L1 fabrics as well as sheath and isoclinal folds under estimated thermobarometric conditions of 790 °C and 1.6 GPa. The pressures and temperatures estimated for D2 are 1.1–1.4 GPa and 705–740 °C, respectively (Puelles et al., 2005a,b). Amphibolite-facies retrogression coeval with localized, low angle D3 shear zones occurred at ca. 375–380 Ma, whereas

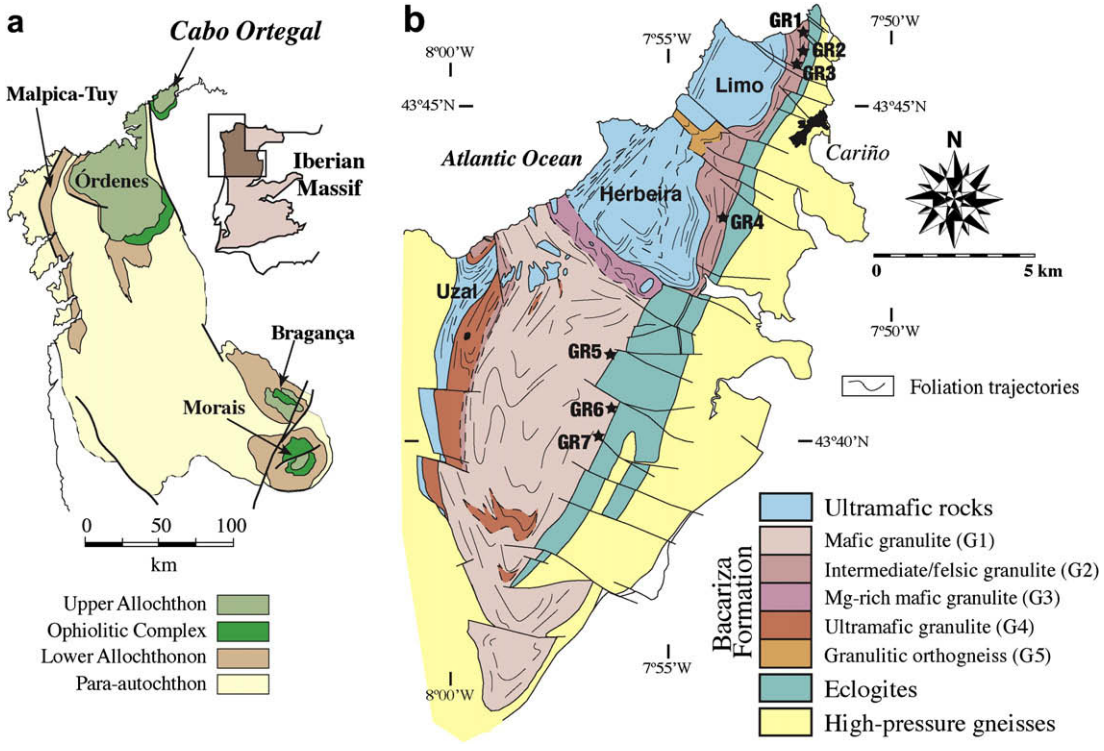

Fig. 1. (a) Geological sketch of NW Iberia showing the units that constitute the Allochthonous Complexes and their para-autochthon. (b) Simplified geological map of the high-pressure rocks of Cabo Ortegal Complex and sample location. Foliation trajectories superimposed to the granulitic lithologies are D1 structures.

greenschist-facies retrogression (giving rise to discrete D4 shears) was dated between ca. 350 and 360 Ma by Peucat et al. (1990) and Dallmeyer et al. (1997).

2.2. D2 shear zones

D2 reworking led to transposition and mylonitization processes that affected the granulites at the contacts with the neighbour peridotite and eclogite formations. The geometrical characteristics of D2 ductile, high-temperature deformation (>700 °C) in the contacts of the high-pressure granulites with the overlying peridotite massif were studied by Puelles et al. (2005b, 2007), whereas a specific study of the rheological behaviour of the D2 contact with the underlying eclogite massif was accomplished by Ábalos et al. (1996), based upon quartz microfabrics.

The structural analysis carried out on the top-bounding upper shear zone showed that S1 was deformed and transposed by S2 foliations defined by a mineral assemblage similar to that of S1. Currently, most of the S2 foliations are sub-horizontal. Their average orientation is 15°/095° and the L2 mineral and stretching lineations plunge ca. 10°/025°. The shear zones concentrate in a hectometre-thick sole under the ultramafic sheet and associate a top-to-the-NNE tectonic displacement of hangingwall blocks. Extremely deformed rocks in close association with these shear zones include planar blankets up to 1 m thick of (1) very fine-grained, seemingly structureless ultramylonitic rocks of fluidal appearance (Puelles et al., 2007), (2) garnet–clinopyroxene-bearing metacarbonate rocks (Santos Zalduegui et al., 1996), and (3) garnet–biotite-rich, usually migmatitic intercalations with restitic parts containing abundant garnet ± biotite and, occasionally, relict clinopyroxene (Puelles, 2004).

The D2 shear zone of the contact with the eclogite massif is dam-thick, dips 50–70° to the WNW and the lineations plunge <15° to the NNE or the SSW. D2 reworked the granulite facies rocks, leading to mylonitization and complete transposition. It progressed from confining pressures of 1.5–1.7 GPa and minimum temperatures of 600 °C under estimated low differential stress (10 MPa) and slow strain rates (10–15–10–13 s^{-1}). Then it continued to minimum temperatures of 520 °C at higher differential stresses (≥25 MPa) and faster strain rates (between 10–14 and 10–12 s^{-1}). The effective viscosity evolved, too, during cooling and deformation localization. Shear zone-parallel displacement rates varied from ca. 0.8 to 8.0 mm/yr and exhumation rates of 0.4–4.1 mm/yr accompanied cooling from 800 ± 45 °C to 325 ± 50 °C at a rate of c. 17 °C/Ma (Ábalos et al., 1996).

2.3. Sample location and petrography

The transposed granulites studied (GR1–GR7; Fig. 1b) were collected close to the contact of the Bacariza Formation with the eclogite massif. Samples GR1–GR4 are also close to the sole of the ultramafic Limo and Herbeira massifs. Samples GR1–4 are intermediate to felsic granulites, whereas samples GR5–7 are mafic granulites. They all are fine-grained mylonitic rocks with a characteristic grey-bluish colour. A compositional banding is parallel to the principal, penetrative foliation recognized at the outcrop and microscopic scales (S2), as well as to the trace of D2 shear zones and the major lithological contacts (Fig. 2a). Centimeter- to meter-thick leucocratic bands are made of plagioclase, quartz, and minor amounts of primary garnet, clinopyroxene and rutile. They alternate with a similar proportion of mafic/ultramafic bands composed of garnet, clinopyroxene and plagioclase.

The microstructures recognized (Fig. 2b–f) vary from oriented granoblastic to porphyroblastic. In the inner parts of the shear zones microstructures are mylonitic to ultramylonitic. The average mineral assemblage in textural equilibrium contains quartz (40%), plagioclase (35%), garnet (15%), augitic clinopyroxene (5%), zoisite/clinozoisite (3%), and minor amounts of rutile and opaque minerals. A retrograde mineral assemblage post-dating D2 fabrics (e.g.: Fig. 2d) includes amphibole (after clinopyroxene, sometimes up to its total replacement), secondary plagioclase (after garnet and clinopyroxene, in this case forming symplectites) and titanite (after rutile and ilmenite). Puelles et al. (2005a) presented a detailed description of the diagnostic primary and secondary textural relationships of these mineral assemblages. The macroscopic S2 and L2 are defined by the shape-preferred orientation of crystals (clinopyroxene, rutile) or mineral aggregates (quartz, plagioclase) of the phases that constitute the stable, primary granulitic mineral assemblage (Fig. 2b and c). Clinopyroxene and garnet crystals or polycrystalline aggregates with sigmoidal morphologies are common (Fig. 2d and e). Elongated garnet crystals in these rocks (Fig. 2e and f) contrast with the widespread equidimensional morphology of this mineral outside the D2 shear zones.

3. Analytical methods

Standard 30 μm thick oriented rock sections were used for conventional petrographic microscopy. The sections were cut parallel to the *XZ* structural planes (*XY*: microscopic foliation plane orientation; *X*: mineral and stretching lineation orientation). Polished sections were used for microprobe analysis. The Electron Black-Scattered Difraction (EBSD) study was performed on selected rock sections ultra-polished to remove sample surface damage. These were prepared with a colloidal silica suspension during polishing periods varying from 6 to 10 h. Samples were covered with an Au–Pa layer before polishing completion to avoid electric charging induced by holes and grain loss after lapping. Carbon coating was avoided to enhance EBSD pattern quality acquisition.

Lattice preferred orientation (LPO) measurements were performed at the University of the Basque Country (Faculty of Science and Technology) with an automated electron-back-scattered diffraction system (Channel5, HKL) attached to a JEOL JSM-7000F Field Emission Scanning Electronic Microscope (FE-SEM). Samples were mounted in this apparatus on a stage tilted 70°, with the rock lineation (structural *X* reference direction) parallel to the SEM *X*-axis. The beam working distance was 15 mm (Prior et al., 1999). A low acceleration voltage of 10 kV, a beam current of ca. 14 nA and a copper tape attached to the sample surface surrounding the measurement area were used to reduce charging effects. Crystallographic orientation solutions with Mean Angular Deviation (MAD) values over 1.2 (between detected and simulated patterns) were rejected to assure EBSD measurement reliability.

Orientation maps and LPOs were obtained using the Channel5 software package after automated EBSD analysis on predefined sampling grid steps of 10–30 μm. These steps are sometimes significantly smaller than the average grain size of some porphyroclastic mineral aggregates and can create artifacts in the pole figure contours. The latter are presented in lower hemisphere, equal area stereographic diagrams. The projection planes always correspond to structural *XZ* sections and, therefore, the macroscopic foliation is represented there as the equatorial diameter (E–W) and the lineation is horizontal within the same plane. Orientation distribution representations in Inverse Pole Figures (IPFs) and the Orientation Distribution Function (ODF) were calculated from the individual orientations using specific Channel5 software packages (the latter using a Gaussian bell curve smoothing width of 20°). The

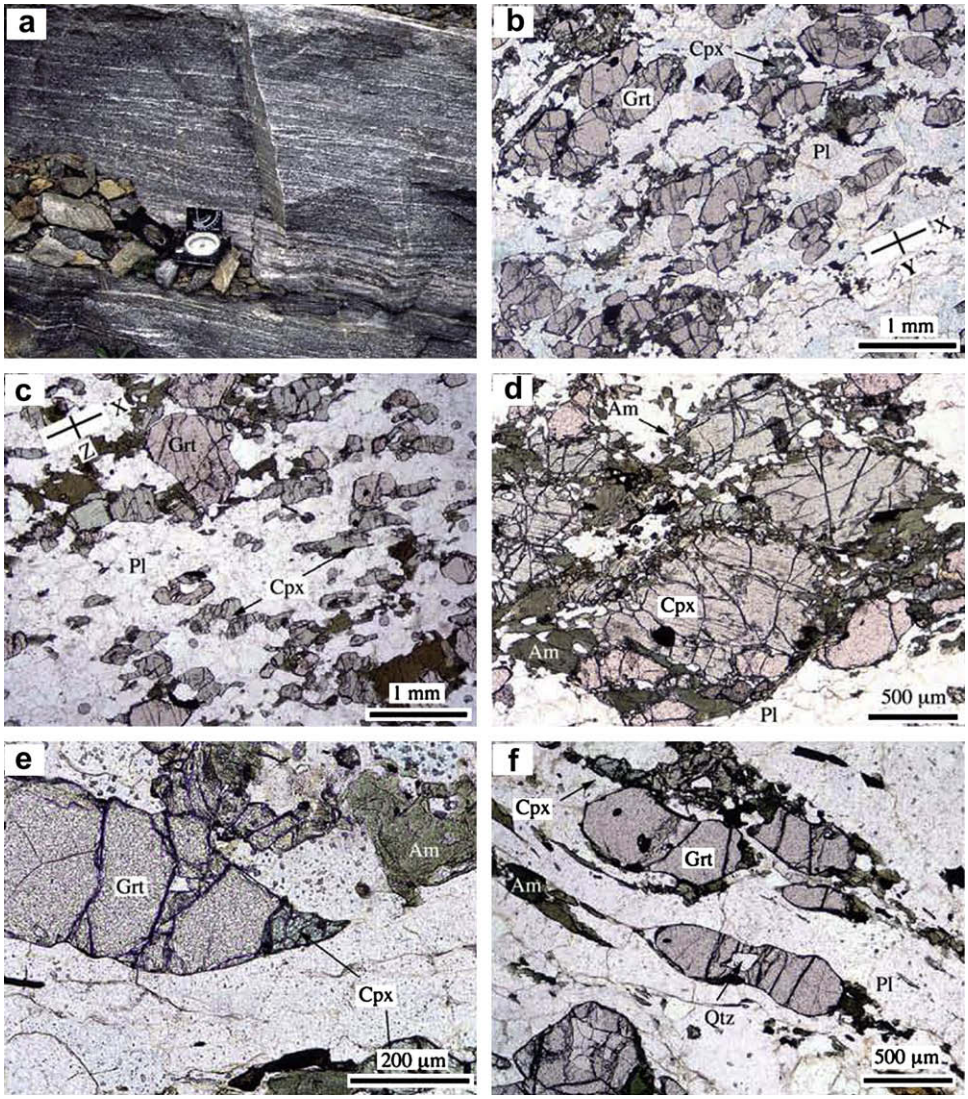

Fig. 2. (a) Field photograph showing S2 compositional banding in intermediate to felsic, plagioclase-rich granulite. (b) Micrograph showing shape-preferred orientation of garnet crystals and aggregates parallel to the macroscopic S2 foliation in a *XZ* structural section (*X*: lineation direction; *XY*: foliation plane). (c) Shape-preferred orientation of clinopyroxene crystals parallel to the macroscopic S2 in a *XZ* structural section. (d) Partly retrogressed, primary clinopyroxene crystals with sigmoidal morphology. Reactional rims are composed of symplectite and amphibole and depict mimetic replacement of a high-pressure assemblage containing omphacitic clinopyroxene, garnet and rutile. (e) Sigmoidal, elongated garnet porphyroclast with a clinopyroxene strain fringe in textural equilibrium. (f) "Pinch and swell"-like morphologies of garnet crystals elongated (stretched) parallel to L2. The strain fringes contain relic clinopyroxene and amphibole. All micrographs were shot under plane polarized light.

strength of the texture was expressed by the texture index *J*, calculated as the mean square value of the ODF.

4. Microstructures and fabrics

The rock samples studied (Fig. 1b) are intermediate to felsic (GR1-4) and mafic (GR5-7) granulites transposed during D2 to mylonitic tectonites. Since garnet, clinopyroxene, plagioclase and quartz form the primary mineral assemblage in equilibrium and their shape fabrics depict resolved geometrical relationships with respect to the D1 and D2 tectonic events, we envisage that their LPOs should reflect the deformation mechanisms operative under the high-pressure granulite facies thermobaric conditions. Secondarily, retrograde minerals such as amphibole and biotite, as well as symplectitic microstructures post-dating the granulitic fabrics provide additional constraints on D2 deformation.

4.1. Garnet

Garnet occurs as porphyroclasts embedded within a quartz–feldspathic matrix with widespread evidence of plastic deformation and recrystallization. Garnet forms ca. 10–15% of the rock with a grain size up to 3.5 mm. The average composition is $Almandine_{43-58}$-$Grossular_{7-29}Pyrope_{11-28}Andradite_{1-9}Spessartine_{1-3}$ (Table 1). Scarce mineral inclusions are usually of equidimensional, strain-free quartz grains, though clinopyroxene, phengite, rutile and opaque mineral grains also occur.

Some garnet grains exhibit in *XZ* structural sections sigmoidal or lensoidal morphologies with narrow necks in the central parts. They resemble "pinch and swell" structures (Fig. 2e–f). The aspect ratio of these grains ranges between 1 and 8, with a mean value of 2. The long garnet axes and the structural *X* direction are subparallel (the angle between them averages -1° when automatically calculated from EBSD maps). The most elongate garnets occur in

Table 1
Representative microprobe analyses and structural formulae of the D2 high-pressure mineral assemblage.

Sample	GR5	GR5	GR6	GR6	GR7	GR7	GR3	GR5	GR6	GR5	GR6	GR7	GR3	GR5	GR6	GR6	GR7	GR7
Mineral	Grt-r	Grt-c	Grt-c	Grt-r	Grt-c	Grt-r	Cpx	Cpx	Cpx	Pl	Pl	Pl	Am	Am	Am	Bt	Bt	Bt
SiO_2	37.5	36.8	37.09	37.32	37.17	37.26	52.58	51.59	52.33	65.8	66.12	64.77	42.67	41.56	41.74	36.74	35.26	34.65
TiO_2	0.00	0.03	0.05	0.01	0.11	0.08	0.23	0.29	0.27	0.00	0.00	0.02	0.89	1.47	0.71	4.10	5.04	4.98
Al_2O_3	21.92	21.54	21.65	22.08	21.39	21.64	10.55	7.74	7.54	21.16	21.3	20.99	15.19	13.6	13.35	16.70	14.47	14.47
Cr_2O_3	0.00	0.00	0.01	0.00	0.00	0.00	0.01	0.01	0.01	0.03	0.00	0.04	0.00	0.1	0.00	bd	bd	bd
FeO	25.71	26.05	28.07	27.82	26.5	26.68	6.17	8.74	9.87	0.16	0.17	0.08	12.1	15.77	16.69	14.11	17.54	17.94
MnO	0.85	0.63	1.36	1.26	1,00	0.87	0.00	0.07	0.06	0.01	0.00	0.01	0.01	0.02	0.26	0.03	0.13	0.08
MgO	5.09	5.53	6.41	6.71	3.06	3.23	9.03	8.96	8.46	0.03	0.04	0.00	12.37	10.44	10.7	13.4	11.28	11.28
CaO	9.12	8.6	5.19	5.33	10.72	10.31	17.09	17.08	16.52	2.35	2.47	2.15	11.02	10.41	10.59	0.00	0.01	0.00
Na_2O	bd	bd	bd	bd	bd	bd	4.48	3.96	4.43	10.26	8.51	9.97	2.44	2.32	2.3	0.13	0.04	0.09
K_2O	bd	bd	bd	bd	bd	bd	0.03	0.01	0.00	0.41	0.41	0.56	1.27	1.2	1.29	9.76	9.46	9.82
Total	100.19	99.17	99.82	100.53	99.95	100.07	100.17	98.44	99.48	100.21	99.02	98.56	97.94	96.88	97.64	94.97	93.23	93.32
O	12	12	12	12	12	12	6	6	6	8	8	8	23	23	23	11	11	11
Si	2.91	2.89	2.9	2.89	2.93	2.93	1.9	1.92	1.93	2.89	2.92	2.89	6.25	6.27	6.29	2.82	2.81	2.78
Ti	–	–	–	–	–	–	0.01	0.01	0.01	<0.01	<0.01	<0.01	0.1	0.17	0.08	0.28	0.30	0.30
Al	2.01	1.99	1.99	2.01	1.99	2.01	0.45	0.34	0.32	1.1	1.11	1.11	2.62	2.42	2.37	1.51	1.51	1.51
Cr	–	0.00	0.00	0.00	0.00	0.00	<0.01	<0.01	<0.01	<0.01	<0.01	<0.01	–	–	–	–	–	–
Fe^{3+}	0.08	0.12	0.1	0.1	0.08	0.06	0.06	0.1	0.12	0.00	0.00	0.00	0.00	0.00	0.00	0.00	0.00	0.00
Fe^{2+}	1.59	1.59	1.73	1.7	1.67	1.7	0.13	0.18	0.18	<0.01	<0.01	<0.01	1.48	1.99	2.1	0.88	1.14	1.17
Mn	0.06	0.04	0.09	0.08	0.07	0.06	<0.01	<0.01	<0.01	–	–	–	<0.01	<0.01	<0.01	0.00	0.01	0.01
Mg	0.59	0.65	0.75	0.77	0.36	0.38	0.49	0.5	0.46	<0.01	<0.01	<0.01	2.7	2.35	2.4	1.53	1.34	1.35
Ca	0.76	0.72	0.43	0.44	0.9	0.87	0.66	0.68	0.65	0.11	0.12	0.1	1.73	1.68	1.71	0.00	0.00	0.00
Na	–	–	–	–	–	–	0.31	0.28	0.32	0.87	0.73	0.86	0.69	0.68	0.67	0.02	0.01	0.02
K	–	–	–	–	–	–	0.00	0.00	0.00	0.02	0.02	0.03	0.24	0.23	0.25	0.96	0.96	1.00

Grt, garnet; Cpx, clinopyroxene; Pl, plagioclase; Am, amphibole; Bt, biotite. c and r: crystal cores and rims.
bd: below detection limits.

quartz-rich layers and do not show compositional zoning or euhedral faces. They are not in equilibrium with biotite or sillimanite, with which they might have reacted pseudomorphically. Polycrystalline quartz–feldspar ribbons adjacent to elongated garnets wrap around them and help to define the macroscopic foliation.

Elongated garnets often display intra-granular, closely spaced straight fractures in *XZ* and *XY* structural sections. In equidimensional garnets two systems appear: one is perpendicular to the lineation and formed by microfractures more planar and regular and the other (not so well-developed) is parallel to the foliation. Other fractures are transgranular (relatively more abundant). The crack surfaces are planar and lack evidence of slip or of ductile deformation at the tips. Garnet fractures oblique to the foliation occur near the granulite–eclogite contact. Crosscutting relationships indicate that they developed after the fractures already described. These are planar or slightly curved cracks and a small amount of slip took place along them (as recognized by Trepmann and Stöckhert, 2002). Most fractures, however, are consistent with tensile mode I cracks. Their orientations, normal to the macroscopic lineation (as also noticed by Prior, 1993 and Ji and Martignole, 1994) suggest that they are controlled by a preferred garnet crystallographic orientation or by the strain geometry associated to D2.

Garnet LPOs determined after indexing EBSD patterns are presented in Fig. 3 for the poles to {100}, {110} and {111} plane families (in fact, for three <100>, six <110> and four <111> symmetrically equivalent crystallographic directions in every single grain). The values of the texture index *J* are very low in the samples studied (1.02–1.09) and, therefore, their LPOs are virtually random. Pole maxima are very weak. Sometimes they are close to the lineation, to the foliation normal, or form part of ill-defined discontinuous girdles, but these patterns are neither systematic nor conclusive. We attempted to identify intracrystalline deformation features in garnet using inverse pole figure maps from sample areas with elongated garnets (Fig. 4). Storey and Prior (2005) and Vollbrecht et al. (2006) used this method to highlight inter- or intra-granular distortions that might imply the occurrence of dislocations and subgrains. Except for one stretched grain made of two subgrains and other rare grains with faint internal domains elongated at a high angle to the foliation (Fig. 4), most of the analysed garnets are internally homogeneous in orientation, suggesting that a single crystal forms each grain.

4.2. Clinopyroxene

Primary clinopyroxene is augite (Q_{67-88}Jadeite$_{7-30}$Aegirine$_{0-11}$; Q: "pyroxene quadrilateral" after Morimoto et al., 1988; Table 1). Ellipsoidal grains define a shape fabric parallel to the rock lineation, with long axes up to 1.75 mm in length and aspect ratios between 2 and 5. Mirostructural evidence indicating crystal-plastic deformation is widespread and includes undulose extinction (Fig. 5a), subgrain boundaries forming high angles with the foliation, kink planes subparallel to the foliation (Fig. 5b), subgrains (Fig. 5c) and microboudinage (Fig. 5d). Sigmoidal porphyroclastic aggregates also occur, in textural equilibrium with garnet and rutile (Fig. 2e). Secondary symplectitic clinopyroxene has an average composition of Q_{81}Jadeite$_{13}$Aegirine$_{6}$. Together with secondary plagioclase, plume-like or vermicular symplectitic aggregates texturally overgrow the primary clinopyroxene, and thus postdate the development of its shape orientation. Symplectites exhibit microtextures so delicate that, had these rocks undergo any deformation after their crystallization under still high temperature and pressure, they would have been destroyed (Godard and Van Roermund, 1995).

Clinopyroxene LPOs (Fig. 6) show poles to {010} forming clear point maxima normal to the macroscopic foliation, whereas the poles of {001} define a girdle perpendicular to the [010] direction and contained within the foliation plane. Two diffuse submaxima of contrasting intensity can be identified in this girdle, one is parallel to the lineation and the other is perpendicular. Crystallographic axes normal to {100} spread in a weak girdle close to the foliation plane. The *J* index yields a texture strength figure of 2.08. The poles of {010} and {001} planes are consistently oblique with respect to the structural reference framework, denoting components of

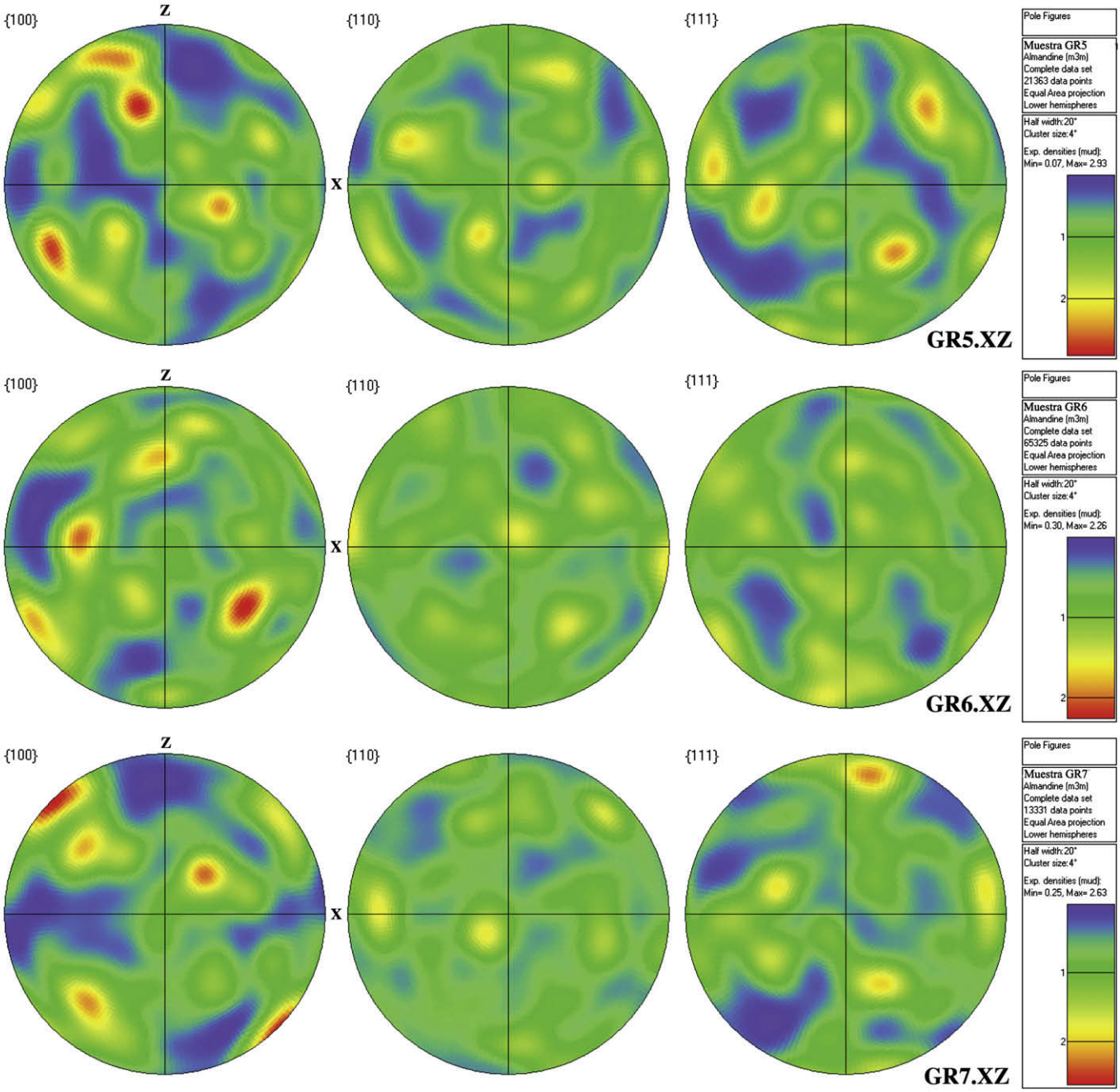

Fig. 3. Orientations of the poles to garnet {100}, {110} and {111} planes. Stereoplot colour patterns represent multiples of mean uniform density.

rotational strain akin to the deduced from asymmetry of sigmoidal crystals or porphyroclast systems.

4.3. Plagioclase

Plagioclase forms a crystal framework made of coalesced porphyroclasts with either granoblastic or core-mantle microstructures. Primary plagioclase porphyroclast cores show deformation twins, subgrains and undulose extinction, whereas recrystallized mantle grains are essentially strain free. Plagioclase composition varies between oligoclase and andesine (Table 1). Porphyroclast cores have an average composition of An_{18}, whereas porphyroclast rims and recrystallized new grains are more calcic (An_{26} and An_{24}, respectively).

Plagioclase LPOs (Fig. 7) are relatively weak and the *J* texture index varies between 1.47 and 1.32. The poles to {100} planes do not show a systematic distribution but tend to scatter in a girdle normal to *Y* (the direction with the minimum data density). The poles to {010} planes define a wide girdle highly oblique to the macroscopic foliation plane. Poles to {001} also define diffuse concentrations close to *Y*.

4.4. Quartz

Quartz, along with feldspar and minor amounts of biotite, is present in disseminated individual crystals of the matrix (with a modal percentage of ca. 40%) or forms polycrystalline ribbons. Quartz ribbons from granulites close to the contact with the

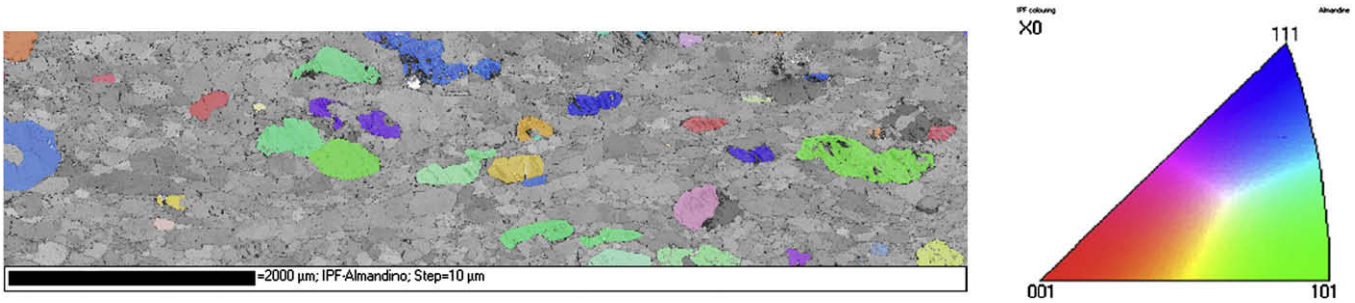

Fig. 4. Garnet inverse pole figure map. Usually there is a homogeneous crystallographic orientation within the grains, which means that each grain is a single crystal. However, various grains in the center of the image contain substructures. See text for further details.

eclogite massif are up to 1 cm thick and a few metres long parallel to the granulite compositional banding and to the principal S2 foliation. Bimodal distributions of grain size and continuous gradations occur in thick quartz ribbons. Quartz grains in the homogeneous ribbons show mean aspect ratios of ca. 2. Maximum aspect rations of 11 can be found in monocrystalline ribbons in *XZ* structural sections. The microstructures observed include: lobulated grain boundaries denoting boundary mobility (Fig. 8a and b), chessboard textures of quartz rectangular grains with boundaries at alternatively high and low angles to the foliation (Fig. 8c), oblique shape fabrics with subgrain boundaries at high angles (up to 65°) to the foliation (Fig. 8c and d), irregular or lobulated grain boundaries and indentations denoting post-deformational grain growth (Fig. 8e) and recrystallized foam microstructures with new grain triple junctions (Fig. 8f) related to the activity of grain surface reduction processes. Undulose extinction and deformation lamellae are often overprinted by high-temperature microstructures associated to grain boundary migration and new grain recrystallization. Recrystallized grain shape fabrics are parallel to the L2 lineation.

Quartz LPOs are characterized by {0001} maxima close to the *Y* structural direction (Fig. 9). These concentrations are not isotropic but slightly elongated between the *Y* and *Z* directions defining either point maxima or more or less diffuse and complete girdles in the *YZ* plane (with submaxima slightly deviated of the *Y* reference axis). The fabric skeletons of these girdles are rotated ca. 30° around *Y*. Poles to {11–20} and {10–10} crystallographic planes define discontinuous girdles at the periphery of the stereoplots with point submaxima near the lineation (*X* direction) or rotated up to 25° with respect to it. Quartz texture strength is characterized by *J* index of 1.4–1.6.

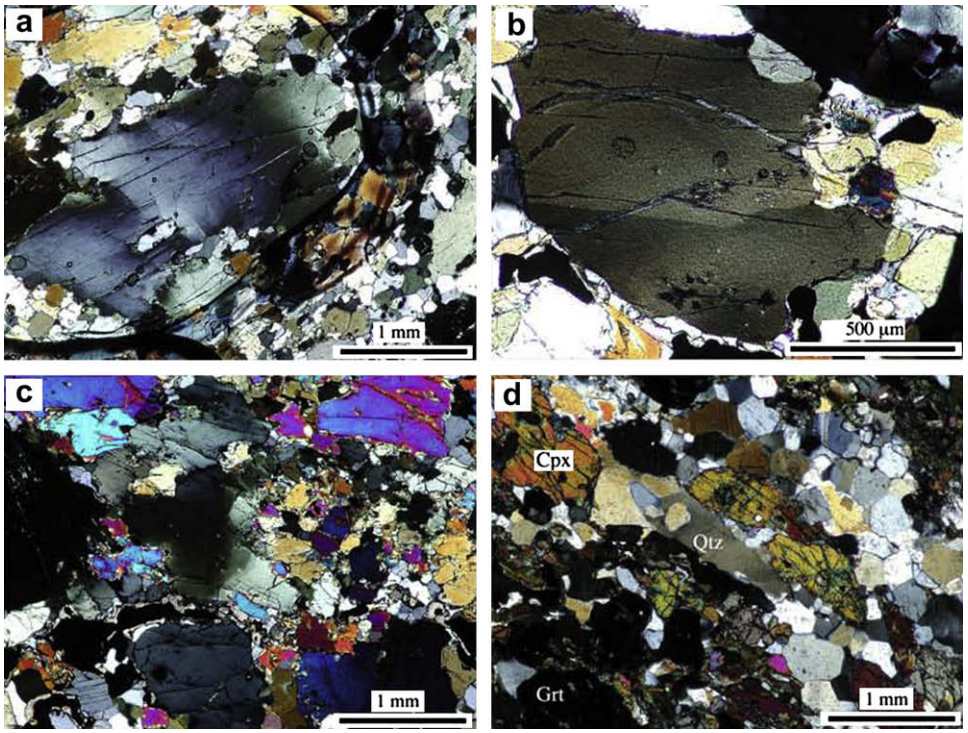

Fig. 5. Clinopyroxene microstructures (all under crossed nicols). (a) Photomicrograph showing undulose extinction in a *XZ* structural section. Note that the clinopyroxene cleavage planes are parallel to the foliation (trending from the upper right corner to the lower left one) and that the undulose extinction bands are subperpendicular to them. (b) Undulose extinction, subgrain boundaries and kink plane development. (c) Clinopyroxene specimen (at the central part of the photomicrograph) with subgrains. (d) Clinopyroxene stretched and boudinaged (parallel to L2) in a dynamically recrystallized quartz–feldspathic matrix. The S2 foliation trends from the upper left corner to the lower right of the microgaph. The original clinopyroxene grain was broken into at least three pieces (labeled 1, 2 and 3).

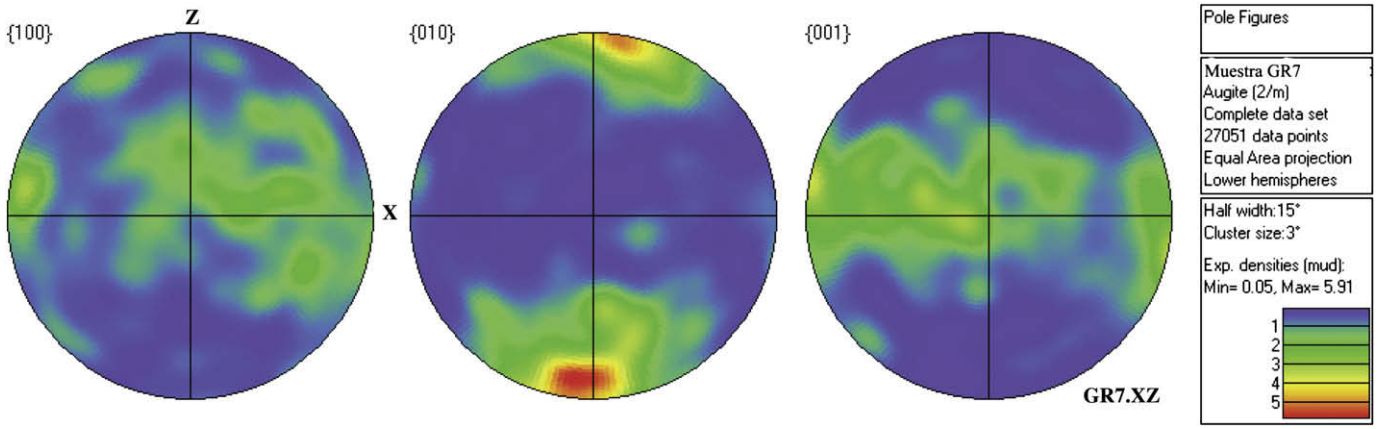

Fig. 6. Orientations of the poles to clinopyroxene {100}, {010} and {001} planes. Stereoplot colour patterns represent multiples of mean uniform density.

4.5. Amphibole

Amphibole is a secondary mineral (see Fig. 2). It occurs either as isolated grains in the matrix or replacing larger clinopyroxene grains, but always shows a shape-preferred orientation subparallel to the D2 macroscopic rock foliation and lineation. In some mylonitized granulites it exhibits mechanical twinning, undulose extinction, subgrains and dynamic recrystallization at the rims of relict clinopyroxene porphyroclasts. Recrystallized new grains have sizes similar to those of the matrix minerals. LPO patterns (Fig. 10) contain a submaximum of the poles to {100} planes close to the *Z* structural direction. {010} pole concentrations define weak girdles normal to the foliation, whereas the axes normal to {001} concentrate close to macroscopic L2.

4.6. Biotite

Biotite crystals occur in the matrix with a modal content of up to 10% and shape-preferred orientations parallel to the rock foliation. They have relatively high X_{Mg} ratios ranging between 0.49 and 0.67 (Table 1). Biotite LPOs (Fig. 11) are strong ($J = 2.99$) and characterized by basal {001} point maxima perpendicular to S2. Poles to

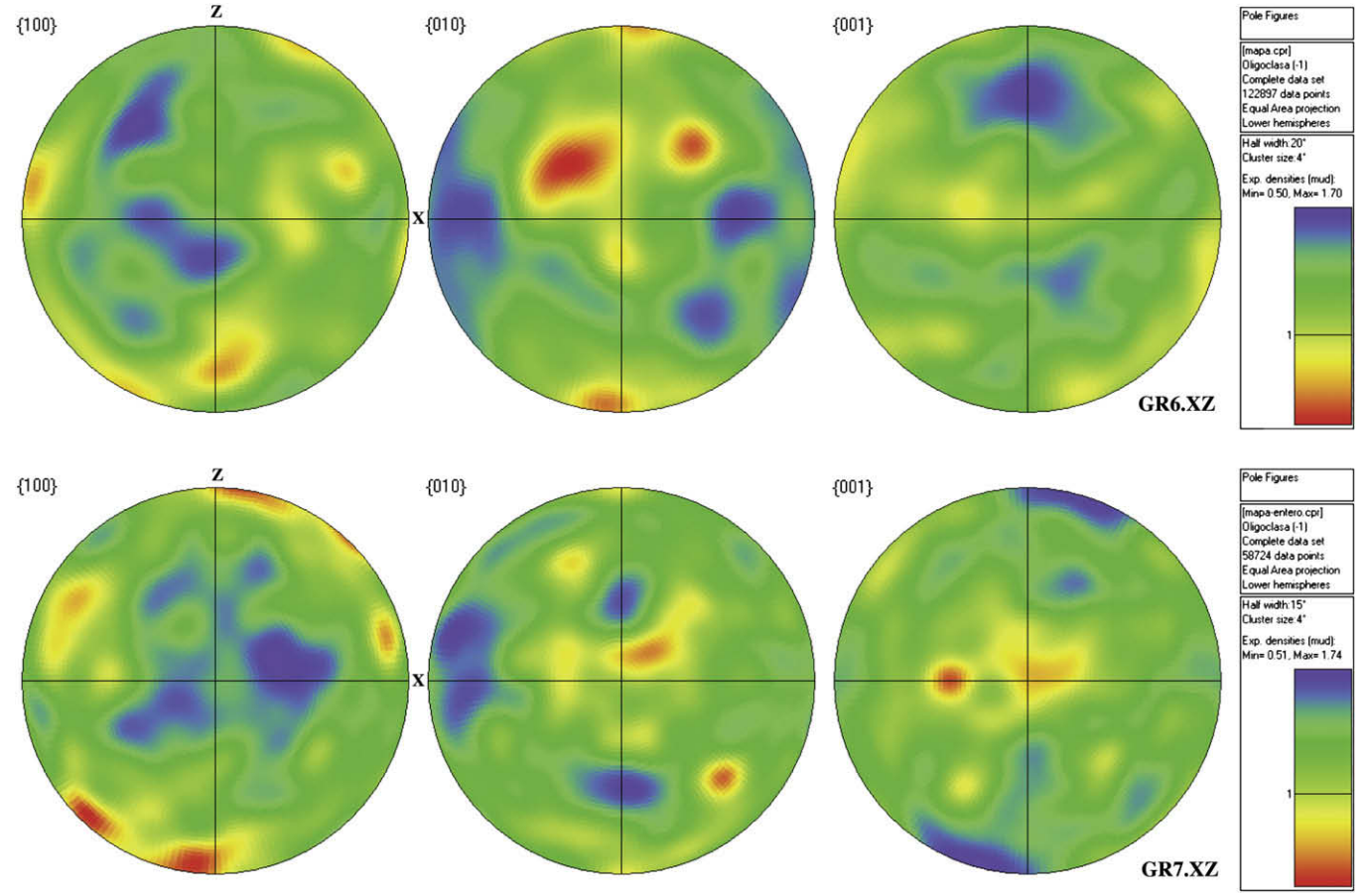

Fig. 7. Orientations of the poles to plagioclase {100}, {010} and {001} planes. Stereoplot colour patterns represent multiples of mean uniform density.

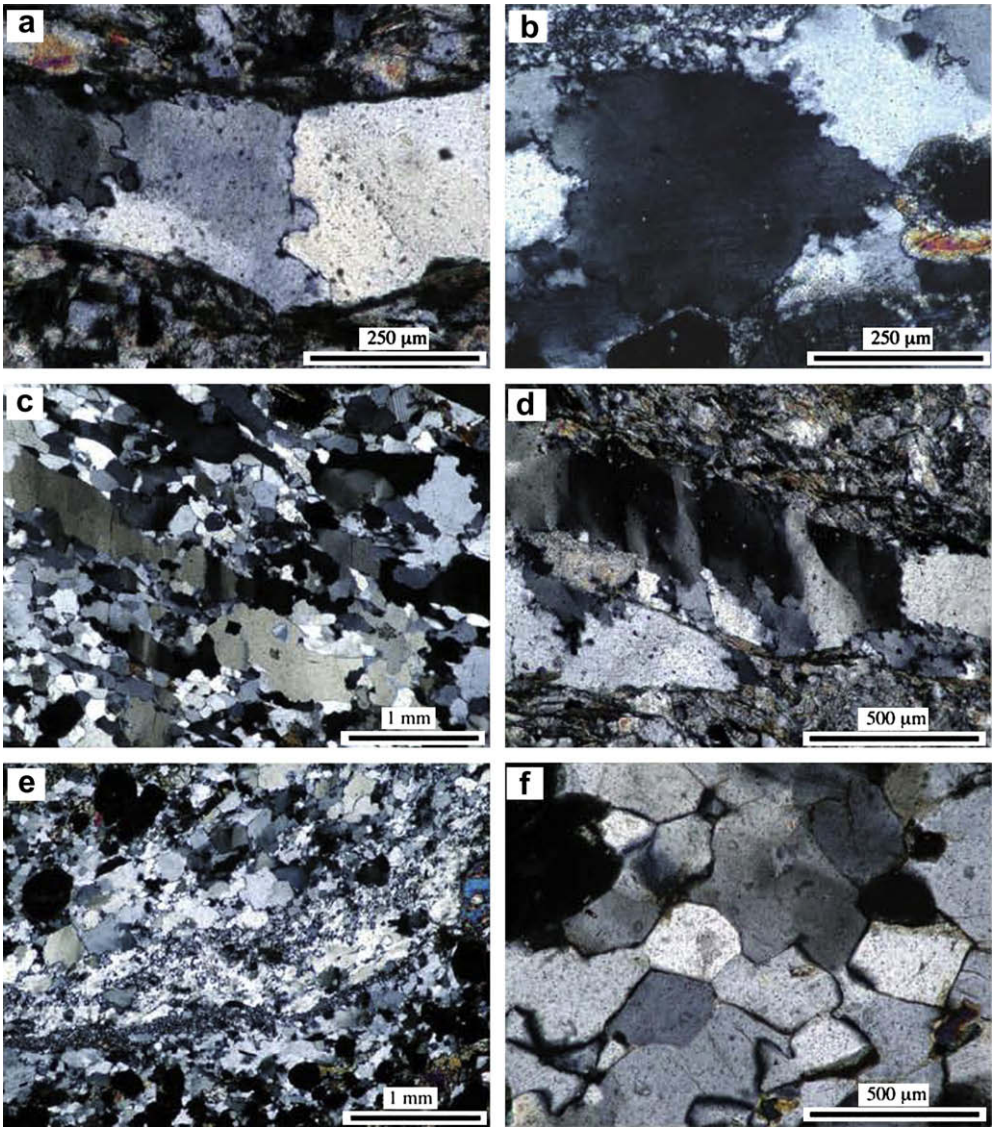

Fig. 8. Quartz microstructures (crossed nicols) in *XZ* structural sections. (a) Polycrystalline quartz ribbon with irregular, lobulated grain boundaries. Undulose extinction and subgrain boundaries oblique to the ribbon length overprint higher-temperature microstructures. (b) Close view of a polycrystalline ribbon (parallel to the microphotograph long axis) showing sub-horizontal deformation lamellae associated with quartz *c*-axes parallel to the L2 lineation. (c) Polycrystalline quartz ribbon with subgrains oblique to the foliation (left part of the micrograph) and chessboard microstructure development (right part of the micrograph). (d) Subgrains and oblique shape fabric development in a polycrystalline ribbon. In this case the orientation of quartz *c*-axes is at a high angle to the foliation. (e) Chessboard-like microstructure. (f) Close view of a quartz polycrystalline ribbon with a dynamically recrystallized "foam" microstructure. Note the occurrence of triple point and straight grain boundaries.

{100} and {010} planes are distributed along more or less continuous girdles subparallel to S2.

5. Discussion

The occurrence of ductile shear zones at the contacts between the high-pressure units studied implies that deformation partitioning and localization played a fundamental role in these movement zones. In the following paragraphs we discuss the implications of the mineral fabrics on deformation partitioning at various scales and deal with the microstructural evidence (complementary to the petrographical mineral assemblages in high-grade/high-pressure metamorphic equilibrium) that permits the unravelling of the associated tectonic displacements which occurred under deep crustal or upper lithospheric mantle thermobaric conditions.

The mineral chemistry of the high-pressure granulite facies rocks studied reflects syn-tectonic equilibration at temperatures of 790–740 °C and pressures of 1.6–1.4 GPa during penetrative D1 and localized D2 shear zone deformations. Microstructures and LPOs of some of the minerals forming the high-pressure assemblage denote the operation of crystal-plastic deformation processes (clinopyroxene, quartz), whereas the evidence is not so clear in garnet, in spite of their deformation related shape fabrics. This is particularly significant from a rheological viewpoint, as at high temperature garnet is expected to reverse its mechanical strength with respect to quartz (Ji and Martignole, 1994).

Garnet often plays a crucial role in recording the thermobaric and geochronological evolution of metamorphic rocks. However, its isotropic character has precluded until recently its consideration in the study of the mechanical behaviour of tectonites. The occurrence of garnet crystals with shape fabrics apparently related to rock deformation has been reported by various authors and studied with

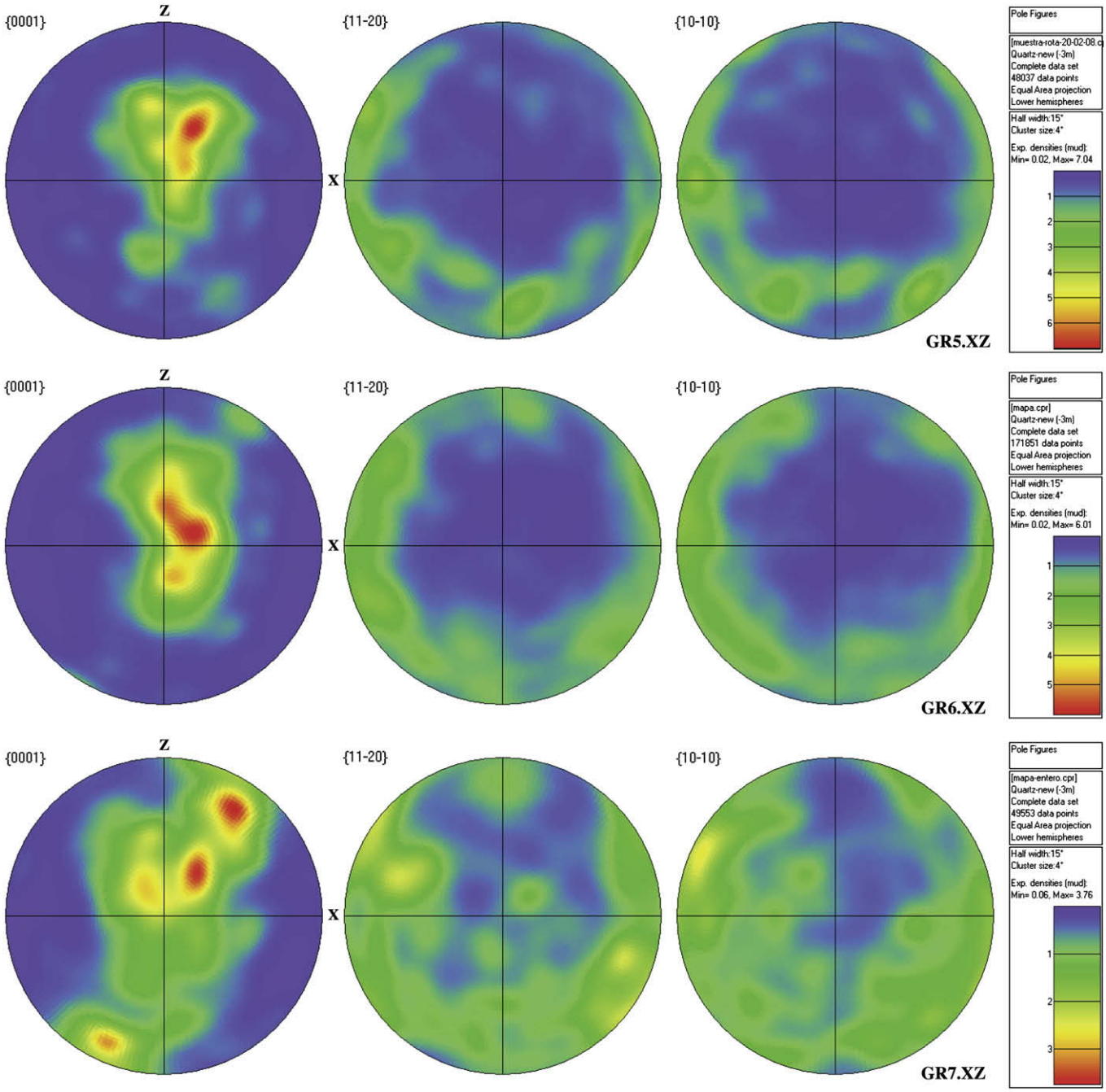

Fig. 9. Orientations of the poles to quartz {0001}, {11–20} and {10–10} planes. Stereoplot colour patterns represent multiples of mean uniform density.

the aid of the techniques available at the time (Dalziel and Bailey, 1968; Mons and Paulitsch, 1970; Voegelé et al., 1998). Recent approaches (Vollbrecht et al., 2006; Whitney et al., 2008) have made use of technologies based on the Scanning Electron Microscope (SEM), notably the electron channelling and electron backscatter diffraction (EBSD; cf. Lloyd, 1987; Prior et al., 1999).

Crystal-plastic deformation mechanisms have often been envisaged to explain the occurrence of metamorphic elongate garnet. Intracrystalline plasticity has been indicated by the presence of dislocations in a wide range of crustal regimes (Ji and Martignole, 1994; Prior et al., 1996; Kleinschrodt and McGrew, 2000; Kleinschrodt and Duyster, 2002; Ji et al., 2003; Storey and Prior, 2005). However, this appears to contradict the relatively low dislocation density often observed in garnets, as well as the rarity of subgrains and its weak LPOs. In high-grade rocks garnet elongation has been explained in terms of plastic deformation under temperature conditions of ca. 800 °C and the diagnostic microstructures cited include garnet boudinage, pinch and swell, flattened and elongate discoidal shapes parallel to the stretching lineation and folded discoidal morphologies. Alternative mechanisms proposed to explain these miscrostructures in high-grade rocks involve principally diffusion flow and anisotropic growth controlled by differential stresses or pre-existing fabrics (Kleinschrodt and McGrew, 2000; Karato and Masuda, 1989).

In principle, the elongated, lensoid garnets with "pinch and swell" microstructures observed in our high-pressure granulite

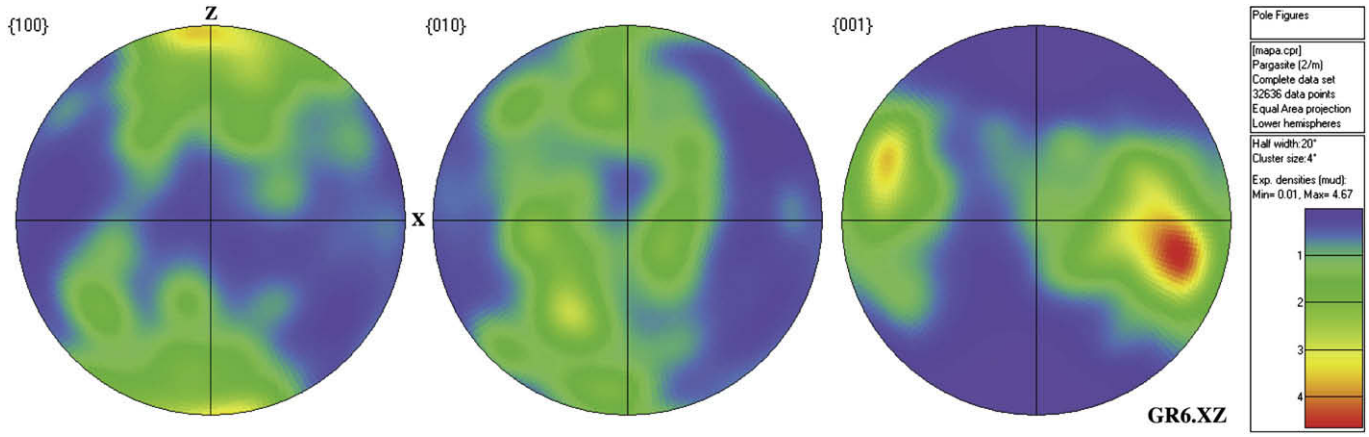

Fig. 10. Orientations of the poles to amphibole {100}, {010} and {001} planes. Stereoplot colour patterns represent multiples of mean uniform density.

samples denote ductile, heterogeneous mineral stretching parallel to the lineation direction. The lack of compositional zoning, zoning truncation or euhedral faces in most elongate garnets and the absence of textural equilibrium with biotite and sillimanite permit us to discard anisotropic growth as a possible mechanism responsible for the observed microstructures, pointing more likely to crystal-plastic deformation processes. Since no systematic LPO pattern was identified in the samples and the textures are weak, we interpret that garnet deformation was controlled by mechanisms producing unsignificant textures (following Vollbrecht et al., 2006) and that the framework-supporting matrix minerals were responsible for the accommodation of part of the bulk deformation. In this regard, the observed wrapping of quartz–feldspar ribbons adjacent to elongated garnets denotes competency contrast between slightly harder garnets and a relatively softer, ribbon matrix supporting the rock framework (Handy, 1990, 1994). Mainprice et al. (2004) also suggested that, though garnet can deform by dislocation creep and recovery, when it is embedded in a matrix of more ductile minerals, the impact of deformation might be lessened or more moderate, as the other minerals accommodate a significant proportion of deformation.

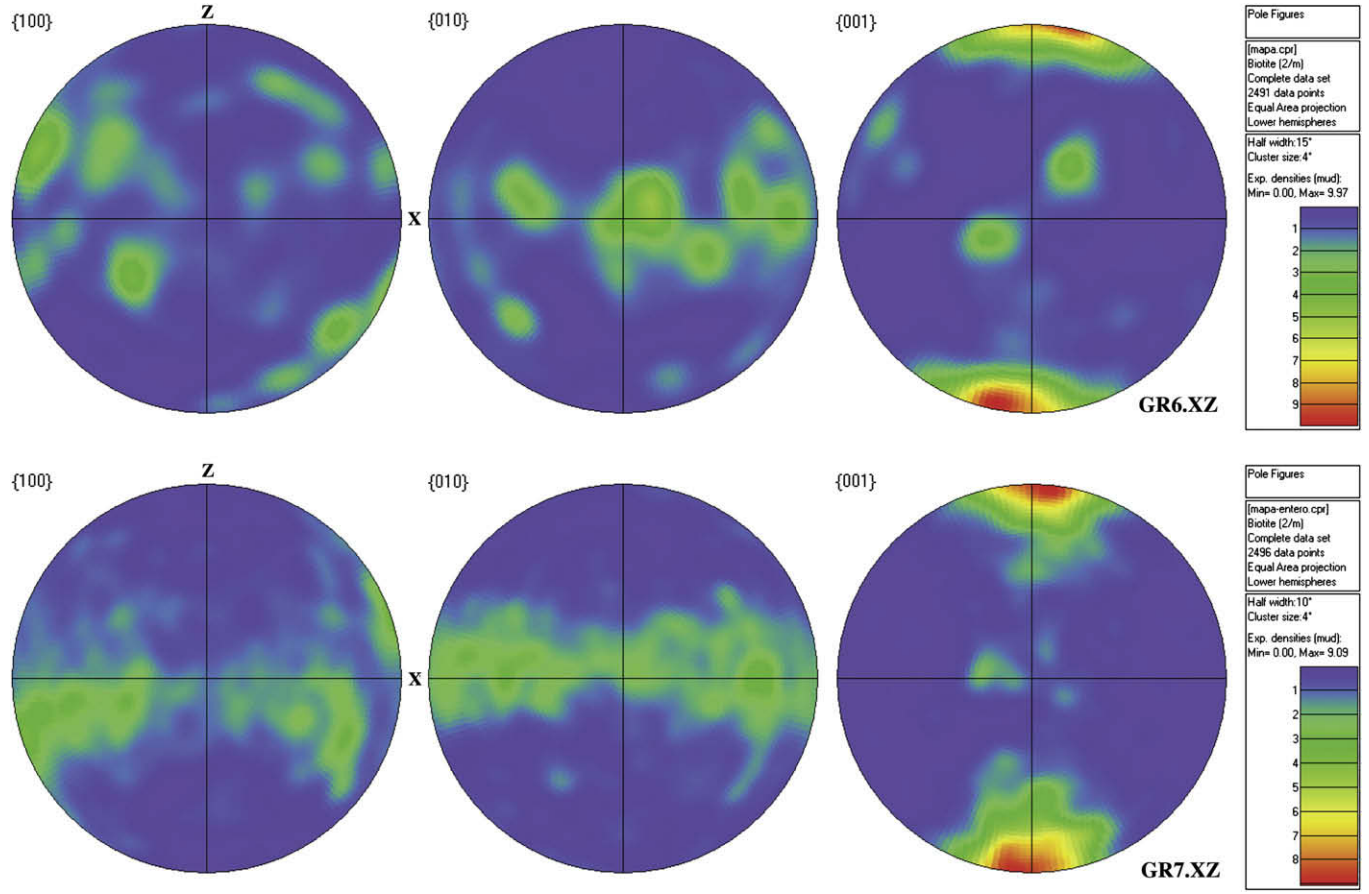

Fig. 11. Orientations of the poles to biotite {100}, {010} and {001} planes. Stereoplot colour patterns represent multiples of mean uniform density.

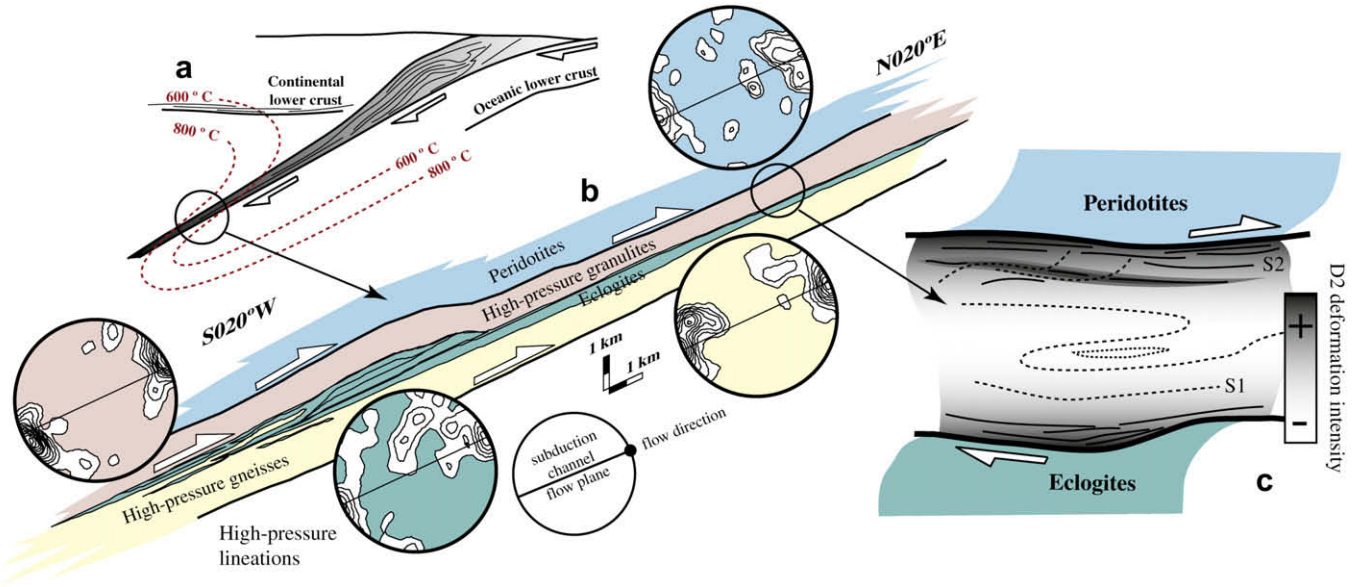

Fig. 12. (a) Sketched model of a moderately dipping subduction zone including the traces of the 600 °C and 800 °C isotherms and of deformed material surfaces in the subduction channel (shaded) after Gerya et al. (2008). (b) Reconstructed section of the upper allochthon of Cabo Ortegal along a projection plane parallel to the regional high-pressure lineation and normal to the foliation. The nappe assemblage 30° dip reflects the apparent dip of a W dipping (steeper) subduction zone along a N020°E relative plate-movement vector. Stereoplots show D1–D2 lineation distributions for the HP Bacariza Formation and bounding units and denote large-scale, syn-metamorphic material flow within the subduction channel. (c) Sketched reconstruction of the Bacariza formation showing reworking and transposition of D1 structures by D2 shear zones.

Crystal-plastic deformation of clinopyroxene is well documented in the literature. LPOs can be used to characterize the strain geometry and kinematics of clinopyroxene-bearing tectonites (Helmstaedt et al., 1972; Boundy et al., 1992; Godard and Van Roermund, 1995) and to relate them to some intracrystalline slip systems (Avé Lallemant, 1978; Buatier et al., 1991). The clinopyroxene LPOs found in this study correspond to the "S-type" of Helmstaedt et al. (1972), that involves various dislocation glide and climb mechanisms (Bystricky and Maxwell, 2001; Mauler et al., 2001; Brenker et al., 2002). Apart from the largest, subhedral clinopyroxene porphyroclasts, some small crystals form pressure fringes around garnet, indicating that the strain geometry controlled clinopyroxene growth, likely assisted by mass transfer. This can influence the LPOs, as a predominance of crystals with [010] axes oriented normal to the foliation and [001] axes parallel to the lineation is favoured by the lower attachment energy of (010) planes and the higher elastic modulus of [001] crystallographic directions (Bass, 1995).

The plagioclase LPOs measured are very weak and systematic patterns can hardly be unravelled. Microscopic evidence supports the simultaneous occurrence of two grain populations (porphyroclastic cores and recrystallized grains, the latter being more abundant). Thus, interpretation of LPOs should involve the recognition of more than one deformation mechanism, one being dominant. The crystallographic fabrics are very weak. Noticeable (010) pole submaxima normal to the lineation and poles to (001) submaxima close to the lineation can be hardly observed. Plagioclase-rich mylonites deformed under amphibolite and granulite facies conditions are often characterized by such patterns, in agreement with experimentally observed prevalence of the [001](010) slip system (Ji et al., 1988; Kruse et al., 2001) enabling dislocation creep. The mixing with other rock supporting minerals such as quartz, as in this case, is often accompanied by weakening of the LPOs. The variations in relative proportions of minerals strongly constrain the aggregate rheological behaviour (Handy, 1990, 1994) and can induce deformation localization. Mehl and Hirth (2008) proposed that the weakness of plagioclase LPOs might also be due to transition to diffusion creep mechanisms involving grain boundary sliding.

The quartz microstructures observed (Fig. 8) are common in experimental high-temperature deformation of quartzites (regime 3 of Hirth and Tullis, 1992). The respective quartz LPOs (Fig. 9) are also common in medium- to high-temperature (amphibolite-facies) mylonites. Point maxima close to *Y* can be interpreted as produced by simple shear-related crystal-plasticity with activation of prism slip (along the [11–20]-axes), whereas point maxima close to *Z* would reflect activation of basal [11–20]-slip (Schmid and Casey, 1986). The onset of lower-grade deformation conditions, of faster strain rates, changing differential stress and strain geometry can explain the details of the LPO variations observed (Law, 1987), as well as its modification by post-tectonic grain growth (Egydio-Silva et al., 2002) or by the occurrence of secondary mineral inclusions (Toy et al., 2008).

Amphibole microstructures suggest that its orientation resulted from epitaxial growth after static replacement of the primary clinopyroxene. Evidence for plastic deformation under greenschist to lower amphibolite-facies conditions is witnessed by mechanical twinning, undulose extinction, and subgrain microstructures (Biermann and Van Roermund, 1983; Brodie and Rutter, 1985; Nyman et al., 1992; Berger and Stünitz, 1996). The LPOs mimic those of clinopyroxene, though they are stronger. Absence of the petrographic relationships described above for these minerals might be interpreted, too, in terms of the activity of [001] slip on (100) crystallographic planes. This slip system has been already detected in naturally deformed amphiboles at temperatures over 650 °C, assisted by dynamic recrystallization. However, several authors have shown that under those conditions, twinning and microfracture processes, as well as diffusion-assisted mechanisms are still operative (Shelley, 1994).

LPO asymmetry with respect to the XYZ reference frame provided by foliation and lineation is clear for the minerals with more obvious, non-random fabrics. The obliquity points to deformation processes with a non-coaxial component in addition to any flattening or constriction. The obliquity degree can also reflect

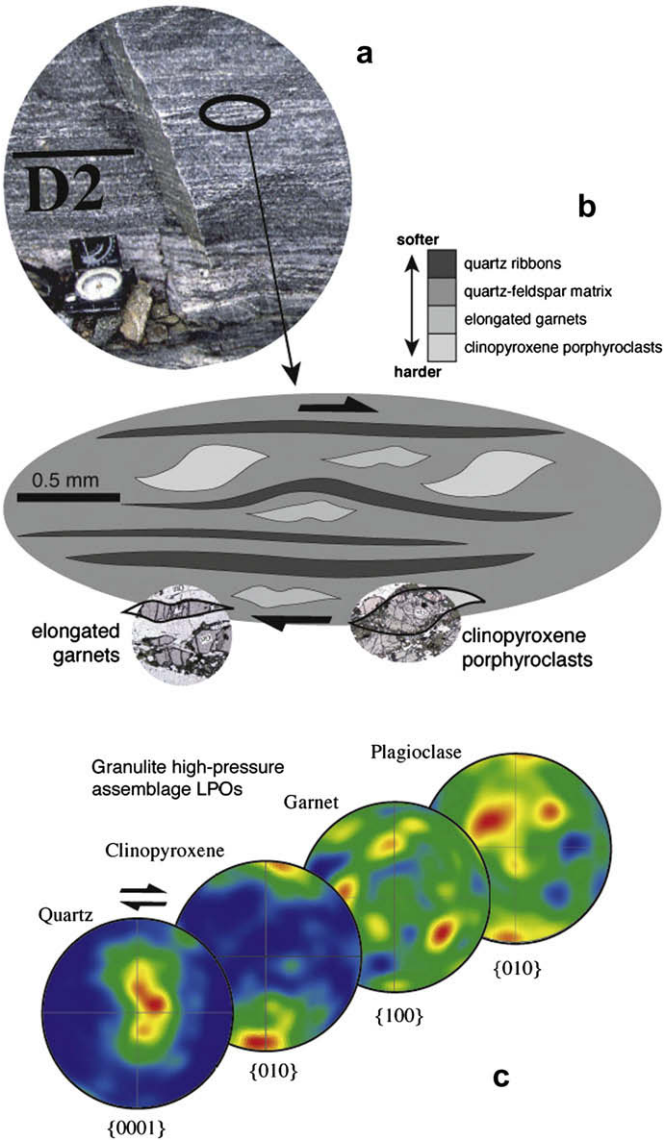

Fig. 13. (a) Field photograph depicting a D2 shear zone with completely reworked high-pressure granulitic mylonite. (b) Petrographic sketch showing the mineral shape fabrics of the components of the granulite facies stable assemblage. A grey-shading code is employed to depict different susceptibilities to crystal-plastic deformation. (c) LPOs of the granulite facies assemblage minerals of D2 mylonites.

variations in the intensity of deformation. The associated shear sense is congruent with the monoclinic symmetry displayed by the porphyroclastic systems and other microstructures, as well as with other outcrop and map scale asymmetric structures (Figs. 12 and 13) always indicating a top-to-the-NNE displacement of hangingwall blocks.

6. Conclusions

The questions discussed enable us to interpret that in the metamorphic and structural contexts of the rocks studied (high-pressure granulite facies in a subduction channel; cf. Fig. 12a) deformation was localized and partitioned at three different scales. These scales sum up to the localization effect of subduction channels at the orogen or lithospheric plate boundary scales.

First, at the map and outcrop scales (Fig. 12b), ductile deformation concentrated along the contacts between the high-pressure granulite formation and the rheologically stronger peridotite and eclogite massifs. The geometrical consequence was the formation of m- to dam-thick ductile shear zones where the pre-existing fabrics were variably transposed (Fig. 12c). The petrological result was the formation of high-pressure granulite facies tectonites, microstructurally different from the original lithologies but with comparable, equilibrium mineral assemblages. Partition of deformation in the contact shear zones led to a contrasting rheological behaviour of the latter (in comparison with the bounding blocks), which accommodated large tectonic displacements under faster strain rates due to its relative weakness. This resulted in a misleading appearance of the shear zones as retrogressive, lower-grade features not directly related to the structural context of the highest-grade units but, perhaps, to its later exhumation under a completely different tectonic regime.

A second level of deformation partition occurred within the shear zones (Fig. 13), where bands of contrasted lithology (more mafic or leucocratic) exhibit contrasting deformation intensities, as it concentrated in the leucocratic layers. The minerals that form these lithologies recorded the thermobaric conditions with varying efficiency, but these remained essentially the same for the whole ensemble and compared to those of the highest-grade rocks acquired during D1. Transposition and reworking of earlier fabrics by the new foliations and lineations (D2) were complete in several instances (Fig. 13a), but microstructural evidence of the older events remains in the form of porphyroclastic mineral assemblages/fabrics. Every lithological layer behaved as a separate rheological unit or mineral aggregate.

A third level of deformation partition occurred within each layer. Layers are often polymineralic and both the microstructures and the LPOs observed denote that crystal-plastic mechanisms dominated mineral deformation (Fig. 13b). This is correct as a big picture and is supported with different confidence levels with the data available, since secondary deformation mechanisms were also active for some minerals. At this level of observation, the microstructures and fabrics can only be used with large uncertainties to deduce the ambient thermobaric conditions of the deformation. Laboratory and field studies data show that they can form without significant variation under temperatures several tens to hundreds of °C different and still under wider pressure intervals. In our case, the only diagnostic microstructures of high-grade deformation of crustal rocks (above 700–800 °C) might be those associated with elongate garnet grain substructures (detected with the EBSD), though with the constraints already discussed. Deformation of a unique mineral assemblage under the same thermobaric conditions also resulted in petrographically different tectonites, depending upon the proportions and rheology of the phases involved. This is relevant for microstructural development of garnet-bearing leucocratic layers and for LPO intensity variation within quartz-feldspar aggregates (Fig. 13c). At temperatures above 700 °C, rheological inversion of garnet and quartz is possible (the quartz becoming harder) as well as the development of plagioclase weak LPOs in spite of the deformation being rather intense.

It is obvious that the high-pressure units studied were exhumed to the surface and that during this process they crossed the thermobaric fields of the lower amphibolite and greenschists facies. The imprint, however, was modest and twofold. On one hand, deformations were concentrated after D2 only along minor (m-scale), narrow and discrete, often low angle, shear zones without a specific structural location. These are the D3 and D4 shears described in a precedent section. On the other hand, the ensemble recorded the imprint of static mineral reactions that begun under relatively high temperatures (enabling symplectite formation) and progressed to lower pressure and temperature without structural transposition.

Acknowledgements

We acknowledge the scientific comments of Drs. K. Brodie and M. Pearce, who helped to improve the quality of the original manuscript. Financial support was provided by the Spanish Ministerio de Ciencia e Innovación ("Grupo Consolidado", project CGL2008-01130/BTE).

References

Ábalos, B., Mendia, M.S., Gil Ibarguchi, J.I., 1994. Structure of the Cabo Ortegal eclogite-facies zone (NW Iberia). Les Comptes rendus de l'Académie des sciences de Paris 319, 1231–1238.

Ábalos, B., Azcárraga, J., Gil Ibarguchi, J.I., Mendia, M.S., Santos Zalduegui, J.F., 1996. Flow stress, strain rate and effective viscosity evaluation in a high-pressure nappe (Cabo Ortegal, Spain). Journal of Metamorphic Geology 14, 227–248.

Ábalos, B., Puelles, P., Gil Ibarguchi, J.I., 2003. Structural assemblage of high-pressure mantle and crustal rocks in a subduction channel (Cabo Ortegal, NW Spain). Tectonics 22 (2), 1006. doi:10.1029/2002TC001405.

Amato, L.M., Johnson, C.M., Baumgartner, L.P., Beard, B.L., 1999. Rapid exhumation of the Zermatt-Saas ophiolite deduced from high-precision Sm–Nd and Rb–Sr geochronology. Earth and Planetary Science Letters 171, 425–438.

Avé Lallemant, H.G., 1978. Experimental deformation of diopside and websterite. Tectonophysics 48, 1–27.

Bascou, J., Tommasi, A., Mainprice, D., 2002. Plastic deformation and development of clinopyroxene lattice-preferred orientation in eclogites. Journal of Structural Geology 24, 1357–1368.

Bass, J.D., 1995. Elasticity of minerals, glasses and melts. In: Ahrens, T.J. (Ed.), Handbook of Physical Constants: Mineral Physics and Crystallography. American Geophysical Union, Washington, pp. 45–63.

Berger, A., Stünitz, H., 1996. Deformation mechanisms and reaction of hornblende: examples from the Bergell tonalite. Tectonophysics 257, 149–174.

Biermann, C., Van Roermund, H.L.M., 1983. Defect structures in naturally deformed clinoamphibole – a TEM study. Tectonophysics 95, 267–278.

Bohlen, S.R., 1991. On the formation of granulites. Journal of Metamorphic Geology 9, 223–229.

Boundy, T.M., Fountain, D.M., Austrheim, H., 1992. Structural development and petrofabrics of eclogite facies shear zones, Bergen Arcs, western Norway: implications for deep crustal deformational processes. Journal of Metamorphic Geology 10, 127–146.

Bousquet, R., 2008. Metamorphic heterogeneities within a single HP unit: overprint effect or metamorphic mix? In: Gerya, T.V., Connolly, J.A.D., Perchuk, L.L. (Eds.), Rocks Generated Under Extreme Pressure and Temperature Conditions: Mechanisms, Concepts, Models. Lithos 103, 46–69. doi:10.1016/j.lithos.2007.09.010.

Brenker, F.E., Prior, D.J., Müller, W.F., 2002. Cation ordering in omphacite and effect on deformation mechanisms and lattice preferred orientation (LPO). Journal of Structural Geology 24, 1991–2005.

Brodie, K.H., Rutter, K.H., 1985. On the relationship between deformation and metamorphism, with special reference to the behavior of basic rocks. In: Thompson, A.B., Rubie, D.C. (Eds.), Metamorphic Reactions: Kinetics, Textures, and Deformation. Springer-Verlag, New York, pp. 139–179.

Buatier, M., Van Roermund, H.L.M., Drury, M.R., Lardeaux, J.M., 1991. Deformation and recrystallization mechanisms in naturally deformed omphacites from the Sesia-Lanzo zone: geophysical consequences. Tectonophysics 195, 11–27.

Burov, E., Jolivet, L., Le Pourhiet, L., Pliakov, A., 2001. A thermomechanical model of exhumation of high pressure (HP) and ultra-high pressure (UHP) metamorphic rocks in Alpine-type collision betls. Tectonophysics 342, 113–136.

Bystricky, M., Maxwell, S., 2001. Creep of dry clinopyroxene aggregates. Journal of Geophysical Research 106, 13443–13454.

Chemenda, A.I., Burg, J.P., Mattauer, M., 2000. Evolutionary model of the Himalaya-Tibet system: geopoem based on new modelling, geological and geophysical data. Earth and Planetary Science Letters 174, 397–409.

Dallmeyer, R.D., Martínez Catalán, J.R., Arenas, R., Gil Ibarguchi, J.I., Gutiérrez Alonso, G., Farias, P., Bastida, F., Aller, J., 1997. Diachronous variscan tectonothermal activity in the NW Iberian Massif: evidence from $^{40}Ar/^{39}Ar$ dating of regional fabrics. Tectonophysics 277, 307–337.

Dalziel, I.W., Bailey, S.W., 1968. Deformed garnets in a mylonitic rock from the Grenville front and their tectonic significance. American Journal of Science 266, 542–562.

Egydio-Silva, M., Vauchez, A., Bascou, J., Hippertt, J., 2002. High-temperature deformation in the Neoproterozoic transpressional Ribeira belt, southeast Brazil. Tectonophysics 352, 203–224.

Ernst, W.G., 2006. Preservation/exhumation of ultrahigh-pressure subduction complexes. Lithos 92, 321–335. doi:10.1016/j.lithos.2006.03.049.

Foreman, R., Andersen, T.B., Wheeler, J., 2005. Eclogite-facies polyphase deformation of the Drøsdal eclogite, Western Gneiss Complex, Norway, and implications for exhumation. Tectonophysics 398, 1–32. doi:10.1016/j.tecto.2004.10.003.

Ganne, J., Marquer, D., Rosenbaum, G., Bertrand, J.M., Fudral, S., 2006. Partitioning of deformation within a subduction channel during exhumation of high pressure rocks: a case study from the Western Alps. Journal of Structural Geology 28, 1193–1207. doi:10.1016/j.jsg.2006.02.011.

Gerya, T.V., Stöckhert, B., Perchuk, A.L., 2002. Exhumation of high-pressure metamorphic rocks in a subduction channel: a numerical simulation. Tectonics 21 (6), 1056. doi:10.1029/2002TC001406.

Gerya, T.V., Perchuk, L.L., Burg, J.P., 2008. Transient hot channels: perpetrating and regurgitating ultrahigh-pressure, high-temperature crust–mantle associations in collision belts. In: Gerya, T.V., Connolly, J.A.D., Perchuk, L.L. (Eds.), Rocks Generated Under Extreme Pressure and Temperature Conditions: Mechanisms, Concepts, Models. Lithos 103, 236–256. doi:10.1016/j.lithos.2007.09.017.

Gil Ibarguchi, J.I., 1995. Petrology of jadeite metagranite and asociated orthogneisses from the Malpica-Tuy Allochthon (NW Spain). European Journal of Mineralogy 7, 403–415.

Gil Ibarguchi, J.I., Ábalos, B., Azcárraga, J., Mendia, M., Puelles, P., 2000. A petrological and structural excursion through the high-grade/high-pressure allochthonous units of the Cabo Ortegal Complex (NW Spain). In: Basement Tectonics 15, Mid-Conference Field Trip, La Coruña, pp. 1–59.

Girardeau, J., Gil Ibarguchi, J.I., Ben Jamaa, N., 1989. Evidence for a heterogeneous upper mantle in the Cabo Ortegal Complex, Spain. Science 245, 1231–1233.

Godard, G., Van Roermund, H.L.M., 1995. Deformation-induced clinopyroxene fabrics from eclogites. Journal of Structural Geology 17, 1425–1443.

Hacker, B.R., Gans, P.B., 2005. Continental collisions and the creation of ultrahigh-pressure terranes: petrology and thermochronology of nappes in the central Scandinavian Caledonides. Geological Society of America Bulletin 117, 117–134. doi:10.1130/B25549-1.

Hacker, B.R., Calvert, A., Zhang, R.Y., Ernst, W.G., Liou, J.G., 2003. Ultrarapid exhumation of ultrahigh-pressure diamond-bearing metasedimentary rocks of the Kokchetav Massif, Kazakhstan? Lithos 70, 61–75. doi:10.1016/S0024-4937(03)00092-6.

Handy, M.R., 1990. The solid-state flow of polymineralic rocks. Journal of Geophysical Research 95, 8647–8661.

Handy, M.R., 1994. Flow laws for rocks containing two non-linear viscous phases: a phenomenological approach. Journal of Structural Geology 16, 287–301.

Helmstaedt, H., Anderson, O.L., Gavasci, A.T., 1972. Petrofabric studies of eclogite, spinel–websterite, and spinel–lherzolite xenoliths from kimberlite-bearing breccia pipes in southeastern Utah and northeastern Arizona. Journal of Geophysical Research 77, 4350–4365.

Hirth, G., Tullis, J., 1992. Dislocation creep regimes in quartz aggregates. Journal of Structural Geology 14, 145–159.

Ji, S., Martignole, J., 1994. Ductility of garnet as an indicator of extremely high temperature deformation. Journal of Structural Geology 16, 985–996.

Ji, S., Mainprice, D., Boudier, F., 1988. Sense of shear in high-temperature movement zones from the fabric asymmetry of plagioclase feldspars. Journal of Structural Geology 10, 73–81.

Ji, S.C., Saruwatari, K., Mainprice, D., Wirth, R., Xu, Z., Xia, B., 2003. Microstructures, petrofabrics and seismic properties of ultra high-pressure eclogites from Sulu region, China: implications for rheology of subducted continental crust and origin of mantle reflections. Tectonophysics 370, 49–76.

Jin, Z.M., Zhang, J., Green II, H.W., Jin, S., 2001. Eclogite rheology: implications for subducted lithosphere. Geology 29, 667–670.

Karato, S., Masuda, T., 1989. Anisotropic grain growth in quartz aggregates under stress and it implication for foliation development. Geology 17, 695–698.

Kleinschrodt, R., Duyster, J.P., 2002. HT-deformation of garnet: an EBSD study on granulites from Sri Lanka, India and the Ivrea Zone. Journal of Structural Geology 24, 1829–1844.

Kleinschrodt, R., McGrew, A., 2000. Garnet plasticity in the lower continental crust: implications for deformation mechanisms based on microstructures and SEM-electron channeling pattern analysis. Journal of Structural Geology 22, 795–809.

Kruse, R., Stünitz, H., Kunze, K., 2001. Dynamic recrystallization processes in plagioclase porphyroclasts. Journal of Structural Geology 23, 1781–1802.

Kurz, W., 2005. Constriction during exhumation: evidence from eclogite microstructures. Geology 33, 37–40. doi:10.1130/G20887.1.

Kurz, W., Neubauer, F., Dachs, E., 1998. Eclogite meso- and microfabrics: implications for the burial and exhumation history of eclogites in the Tauern Window (Eastern Alps) from P–T–d paths. Tectonophysics 285, 183–209.

Kylander-Clark, A.R.C., Hacker, B.R., Mattinson, J.M., 2008. Slow exhumation of UHP terranes: titanite and rutile ages of the Western Gneiss Region, Norway. Earth and Planetary Sience Letters 272, 531–540. doi:10.1016/j.epsl.2008.05.019.

Law, R.D., 1987. Crystallographic fabrics and deformation histories. Journal of the Geological Society, London 144, 675–676.

Lenze, A., Stöckhert, B., 2007. Microfabrics of UHP metamorphic granites in the Dora Maira Massif, western Alps – no evidence of deformation at great depth. Journal of Metamorphic Geology 25, 461–475. doi:10.1111/j.1525-1314.2007.00707.x.

Lenze, A., Stöckhert, B., Wirth, R., 2005. Grain scale deformation in ultra-high-pressure metamorphic rocks – an indicator of rapid phase transformation. Earth and Planetary Science Letters 229, 217–230. doi:10.1016/j.epsl.2004.10.012.

Lloyd, G.E., 1987. Atomic number and crystallographic contrast images with SEM: a review of back-scattered electron techniques. Mineralogical Magazine 51, 3–19.

Mainprice, D., Bascou, J., Cordier, P., Tommasi, A., 2004. Crystal preferred orientations of garnet: comparison between numerical simulations and electron back-scattered diffraction (EBSD) measurements in naturally deformed eclogites. Journal of Structural Geology 26, 2089–2102. doi:10.1016/j.jsg.2004.04.008.

Martínez Catalán, J.R., Arenas, R., Díaz-García, F., Abati, J., 1997. Variscan accretionary complex of northwest Iberia: terrane correlation and succession of tectonothermal events. Geology 25, 1103–1106.

Mauler, A., Godard, G., Kunze, K., 2001. Crystallographic fabrics of omphacite, rutile and quartz in Vendée eclogites (Armorican Massif, France). Consequences for deformation mechanisms and regimes. Tectonophysics 342, 81–112.

Mehl, L., Hirth, G., 2008. Plagioclase preferred orientation in layered mylonites: evaluation of flow laws for the lower crust. Journal of Geophysical Research 113, B05202. doi:10.1029/2007JB005075.

Mons, W., Paulitsch, P., 1970. Garnet orientations in different metamorphic facies. In: Experimental and Natural Rock Deformation. Springer, Berlin, pp. 100–108.

Morimoto, N., Fabriès, J., Ferguson, A.K., Ginzburg, I.V., Ross, M., Seifert, F.A., Zussman, J., Aoki, K., Gottardi, G., 1988. Nomenclature of pyroxenes. Mineralogy and Petrology 39, 55–76.

Neufeld, K., Ring, U., Heidelbach, F., Dietrich, S., Neuser, R.D., 2008. Omphacite textures in eclogites of the Tauern Window: implications for the exhumation of the Eclogite Zone, Eastern Alps. Journal of Structural Geology 30, 976–992. doi:10.1016/j.jsg.2008.03.010.

Nyman, M.W., Law, R.D., Smelik, E., 1992. Cataclastic deformation mechanism for the development of core-mantle structures in amphibole. Geology 20, 455–458.

O'Brien, P.J., Rötzler, J., 2003. High-pressure granulites: formation, recovery of peak conditions and implications for tectonics. Journal of Metamorphic Geology 21, 3–20.

Ordóñez, B., Gebauer, D., Schäfer, H.J., Gil Ibarguchi, J.I., Peucat, J.J., 2001. A single Devonian subduction event for the HP/HT metamorphism of the Cabo Ortegal Complex within the Iberian Massif. Tectonophysics 332, 359–385.

Peucat, J.J., Bernard-Griffiths, J., Gil Ibarguchi, J.I., Dallmeyer, R.D., Menot, R.P., Cornichet, J., Iglesias Ponce de León, M., 1990. Geochemical and geochronological cross section of the deep variscan crust: the Cabo Ortegal high-pressure nappe (NW Spain). In: Matte, Ph. (Ed.), Terranes in the Variscan Belt of Europe and Circum-Atlantic Paleozoic Orogens. Tectonophysics 177, 263–292.

Prior, D.J., 1993. Subcritical fracture and associated retrogression of garnet during mylonitic deformation. Contributions to Mineralogy and Petrology 113, 545–556.

Prior, D.J., Trimby, P.W., Weber, U.D., Dingely, D.J., 1996. Orientation contrast imaging of microstructures in rocks using forescatter detectors in the scanning electron microscope. Mineralogical Magazine 60, 859–869.

Prior, D.J., Boyle, A.P., Brenker, F., Cheadle, M.C., Day, A., Lopez, G., Potts, G.J., Reddy, S., Spiess, R., Timms, N., Trimby, P., Wheeler, J., Zetterstrom, L., 1999. The application of electron backscatter diffraction and orientation contrast imaging in the SEM to textural problems in rocks. American Mineralogist 84, 1741–1759.

Puelles, P., 2004. Deformación, metamorfismo y exhumación de las granulitas de alta presión de la Bacariza (Complejo de Cabo Ortegal, NO de España). Nova Terra 23, 1–411.

Puelles, P., Ábalos, B., Gil Ibarguchi, J.I., 2005a. Metamorphic evolution and thermobaric structure of the subduction-related Bacariza high-pressure granulite formation (Cabo Ortegal Complex, NW Spain). Lithos 84, 125–149. doi:10.1016/j.lithos.2005.01.009.

Puelles, P., Mulchrone, K., Ábalos, B., Gil Ibarguchi, J.I., 2005b. Structural analysis of high-pressure shear zones (Bacariza Formation, Cabo Ortegal, NW Spain). Journal of Structural Geology 27, 1046–1060. doi:10.1016/j.jsg.2005.03.002.

Puelles, P., Ábalos, B., Gil Ibarguchi, J.I., 2007. Microstructural evidence for thermal runaway and deep paleoseismic activity (Cabo Ortegal, NW Spain). Terra Nova 19, 219–224. doi:10.1111/j.1365-3121.2007.00738.x.

Santos Zalduegui, J.F., Schärer, U., Gil Ibarguchi, J.I., 1996. Isotope constraints on the age and origin of magmatism and metamorphism in the Malpica-Tuy Allochthon. Chemical Geology 121, 91–103.

Santos Zalduegui, J.F., Schärer, U., Gil Ibarguchi, J.I., Girardeau, J., 2002. Genesis of pyroxenite-rich peridotite at Cabo Ortegal (NW Spain): geochemical and Pb–Sr–Nd isotope data. Journal of Petrology 43, 17–43.

Schäfer, H.J., Gebauer, D., Gil Ibarguchi, J.I., Peucat, J.J., 1993. Ion-microprobe U–Pb zircon dating on the HP/HT Cabo Ortegal Complex (Galicia, NW Spain): preliminary results. Terra Nova Abstracts 5 (Suppl. 4), 22.

Schmid, S.M., Casey, M., 1986. Complete fabric analysis of some commonly observed quartz c-axis patterns. In: Hobbs, B.E., Heard, H.C. (Eds.), Mineral and Rock Deformation: Laboratory Studies. Geophysical Monograph, vol. 36. American Geophysical Union, pp. 263–286.

Shelley, D., 1994. Spider texture and amphibole preferred orientation. Journal of Structural Geology 16, 709–717.

Storey, C.D., Prior, D.J., 2005. Plastic deformation and recrystallization of garnet: a mechanism to facilitate diffusion creep. Journal of Petrology 46, 2593–2613. doi:10.1093/petrology/egi067.

Terry, M.P., Robinson, P., 2004. Geometry of eclogite-facies structural features: implications for production and exhumation of ultrahigh-pressure and high-pressure rocks, Western Gneiss Region, Norway. Tectonics 23, TC2001. doi:10.1029/2002TC001401.

Tilton, G.R., Ames, L., Schertl, H.P., Schreyer, W., 1997. Reconnaissance isotopic investigations on rocks of an undeformed granite contact within the coesite-bearing unit of the Dora Maira Massif. Lithos 41, 25–36.

Toy, V., Prior, D.J., Norris, R.J., 2008. Quartz fabrics in the Alpine Fault mylonites: influence of pre-existing preferred orientations on fabric development during progressive uplift. Journal of Structural Geology 30, 602–621. doi:10.1016/j.jsg.2008.01.001.

Trepmann, C., Stöckhert, B., 2002. Cataclastic deformation of garnet: a record of synseismic loading and postseismic creep. Journal of Structural Geology 24, 1845–1856.

Voegelé, V., Ando, J.I., Cordier, P., Liebermann, R.C., 1998. Plastic deformation of silicate garnet I. High-pressure experiments. Physics of the Earth and Planetary Interiors 108, 305–318.

Vogel, D.E., 1967. Petrology of an eclogite- and pyrigarnite-bearing polymetamorphic rock complex at Cabo Ortegal, NW Spain. Leidse Geologische Mededelingen 40, 121–213.

Vollbrecht, A., Pawlowski, J., Leiss, B., Heinrichs, T., Seidel, M., Kronz, A., 2006. Ductile deformation of garnet in mylonitic gneisses from the Münchberg Massif (Germany). Tectonophysics 427, 153–170. doi:10.1016/j.tect.2006.05.024.

Wallis, S.R., Ishiwatari, A., Hirajima, T., Ye, K., Guo, J., Nakamura, D., Kato, T., Zhai, M., Enami, M., Cong, B., Banno, S., 1997. Occurrence and field relationships of ultrahigh-pressure metagranitoid and coesite eclogite in the Su-Lu terrane, eastern China. Journal of the Geological Society, London 154, 45–54.

Whitney, D., Goergen, E., Ketcham, R., Kunze, K., 2008. Formation of garnet polycrystals during metamorphic crystallization. Journal of Metamorphic Geology 26, 363–383. doi:10.1111/j.1525-1314.2008.00763.x.

Yamato, P., Burov, E., Agard, P., Le Pourhiet, L., Jolivet, L., 2008. HP–UHP exhumation during slow continental subduction: self-consistent thermodinamically and thermomechanically coupled model with application to the Western Alps. Earth and Planetary Science Letters 271, 63–74. doi:10.1016/j.epsl.2008.03.049.